LAWRENCE
LIVERMORE
NATIONAL
LABORATORY

LLNL-JRNL-844653

Experimental and theoretical study of weakly coherent mode in I-mode edge plasmas in the EAST tokamak

Z. X. Liu, Y. J. Liu, J. Y. Xiao, T. Y. Xia, Y. L. Li, X. Q. Xu

February 1, 2023

Nuclear Fusion

Disclaimer

Experimental and theoretical study of weakly coherent mode in I-mode edge plasmas in the EAST tokamak

Z.X. Liu[1,a,*], Y.J. Liu[1,a], J.Y. Xiao[1], T.Y. Xia[2], Y.L. Li[1,2], X.Q. Xu[3], M.Q. Wu[4], G.Q. Li[2], M.F. Wu[1,2], T. Zhang[2], X. Gao[2], X.Z. Gong[2], H.Q. Liu[2], Q. Zang[2], A.D. Liu[1], C. Zhou[1], T. Lan[1], H. Li[1], J.L. Xie[1], W.Z. Mao[1], W.X. Ding[1], G. Zhuang[1], J.G. Li[2], W.D. Liu[1] and the EAST Team[b]

[1] School of Nuclear Science and Technology, University of Science and Technology of China, Anhui, Hefei 230026, China

[2] Institute of Plasma Physics, Chinese Academy of Sciences, Hefei 230031, China

[3] Lawrence Livermore National Laboratory, Livermore, California 94550, United States of America

[4] Advanced Energy Research Center, Shenzhen University, Shenzhen 518060, China

E-mail: zxliu316@ustc.edu.cn

Abstract

The I-mode is a promising operation mode for fusion in the future, featuring high-temperature and low-density confinement, but the reason why the temperature and density are decoupled remains an important aspect to be explored. The experimental results from the experimental advanced superconducting tokamak (EAST) showed that the weakly coherent mode (WCM) is directly related to sustaining the I-mode and that the peak amplitude of the WCM is proportional to the temperature in the pedestal. Simulating the experimental data from EAST with the six-field model of BOUT++, we find a density perturbation close to the frequency of the WCM observed in the experiment. By testing all the physical terms in this model, we find that the density perturbation and particle transport are directly related to the drift *Alfvén* wave (DAW) mode. We also use the SymPIC program (Xiao *et al Plasma Sci. Technol.* **20** 110501; *Phys. Plasmas* **22** 112504; *Plasma Sci. Technol.* **23** 055102) to simulate the same experimental data and find that the frequency range of the WCM is close to both experimental and BOUT++ results. Therefore, the WCM of the I-mode can be considered to be driven by the DAW, which helps improve the transport of the I-mode.

Keywords: I-mode, DAW, WCM, EAST

1. Introduction

The I-mode is an improved confinement regime for magnetic confinement nuclear fusion, featuring an H-mode-like temperature barrier and an L-mode-like particle barrier [4]. In this way, the I-mode achieves high energy confinement and low particle confinement and can avoid the accumulation of impurities and He 'ash'. In addition, the I-mode is naturally stable against edge-localized modes [5], which are unacceptable in future fusion reactors due to the transient heat pulses to the divertor on an ITER-like scale [6]; thus, the I-mode is an excellent regime for future nuclear fusion research.

* Author to whom any correspondence should be addressed.

The I-mode has been observed since the late 1990s [7] and has been experimentally studied over a wide range of parameters in a few tokamak devices [8–11]. Generally, the I-mode is achieved with ion $B \times \bigtriangledown B$ drift pointing away from the active X-point; this direction is termed 'unfavorable'. Previous research shows that turbulent energy is transformed to zonal flow in the favorable direction, while it is transformed to the geodesic acoustic mode (GAM) in the unfavorable direction [12]. The power threshold for the L–I transition is lower than that of the L–H transition in the unfavorable direction but higher than that of the L–H transition in the favorable direction. Different from that of the H-mode, the power threshold of the L–I transition varies weakly with B_T, while the power range for the I-mode increases significantly with increasing B_T. In addition, almost all known I-mode regimes have been observed to be accompanied by the weakly coherent mode (WCM) [13–15]. The physical mechanism of the decoupling of the transport of energy and particles is not completely clear. A previous work [16] provided the density fluctuations characteristic of a drift wave; when drift-turbulence develops, large- and small-scale fluctuations are suppressed by phase randomization and finite-Larmor-radius effects, respectively; hence, mesoscale fluctuations are developed and form the WCM. In that paper, Manz *et al* concluded that the T_e fluctuations a re d issipated b y e lectron t hermal conductivity, leading to a reduction in electron heat transport; thus, the transport of energy and particles is decoupled. However, in addition to the mechanism that changes only the temperature barrier, it is also possible that interchange-driven turbulence impacts all channels but that something helps improve particle transport. Moreover, the E_r well of the I-mode is found to be between that of the L-mode and that of the H-mode [17, 18]; thus, the weaker E_r well might help form edge barriers such as those in the H-mode. In previous gyrokinetic simulation work using GENE [19], WCM is found to be an electrostatic ion temperature gradient/impurity density gradient (ITG/impurity) driven mode. But the I-mode discharges on EAST we do not observe obvious relationship between WCM and impurities. The I-mode discharges discussed in this paper are divided into two types, one is a stable density and temperature platform is formed immediately with entering the I-mode, the plasma changes with the changing heating power, termed type 1; another is an unstable I-mode, plasma changes with the same heating power, termed type 2, summarized in below table (table 1).

Table 1. Parameter summary.

	Shots	I_p (kA)	B_T (T)	n_e (10^{19} m^{-3})
Type 1	88	0.45 ∼ 0.6	2.241 ∼ 2.521	2.16 ∼ 3.51
Type 2	27	0.45 ∼ 0.6	2.243 ∼ 2.492	2.08 ∼ 3.42

2. Experiment results

Figure 1 shows the time trace of experimental advanced superconducting tokamak (EAST) discharge #86541 as the plasma evolves from the I-mode into the H-mode at 3.7 s. This is a type 1 I-mode as mentioned in the end of introduction. Before the second neutral-beam injection (NBI) injection, the density and electron temperature is stable, also the amplitude of WCM, as shown in figure 1(d) panels. Figure 1(d) panels show the time-frequency spectrum from the four positions from the Doppler reflectometer (DR) system [22], the corresponding positions of figure 1 (d) panels are from top to bottom, from inside to outside. The second NBI was injected at 3.52 s, slight increase in plasma density (1.2% $\Delta n_e/n_e$ change between 3.501 s and 3.536 s in core while 0.5% in edge) and a strong increase in electron temperature (6.6% change between 3.501 s and 3.536 s), with a temporary increase in the intensity of the WCM. Then I–H transition occurred in 3.7 s, with increase in both density and electron temperature, it is also accompanied by the disappearance of WCM.

After the second NBI injection, although plasma is still in I-mode, its status has obviously changed, specially the intensity of WCM. To further study the characteristic of the WCM on the I-mode, a more detailed power spectrum of the DR is exhibited in figure 2. Compare the plasma before and after NBI injection at 3.7 s, the peak amplitude of the WCM in the position of 72.5 GHz reaches twice that of before, and that in the position of 70 GHz reaches 1.7 times that of before, and the amplitude of edge temperature ring oscillation (ETRO [20]) similar to that of WCM. ETRO is a characteristic mode observed in EAST featured poloidal and toroidal symmetry, caused by the turbulence change between an electron diamagnetic drift turbulence (ET) and an ion diamagnetic drift turbulence (IT). The diagnostic positions for four DR channels are shown in figure 2(b), it also shows the radial profiles for pressure of before and after second NBI injection in red and blue line respectively. From the pressure profile, we found the position of 72.5 GHz is in the pedestal range, so the change in the position is closely related to the transport that strongly affects the pedestal condition. However, there is another kind of instabilities shown in the power spectrum, and the possibility exists of the GAM affecting the I-mode. Consequently, the peak amplitude and position of the GAM are studied in figure 2(c3). The amplitude of the GAM decreases, and the position of its peak amplitude moves to the core range rather than the pedestal range.

In discharge #86541, additional power is injected into a stable I-mode; how the WCM affects the unstable I-mode and how it affects the energy source of the WCM are unknown but could help us understand the physical mechanism of the WCM remaining in the I-mode. Figure 3 shows an example of type 2 I-mode, i.e. a discharge remaining in the I-mode for 0.32 s with changing density and the same injection power. In #75366, the lower hybrid wave (LHW) power is kept at 1.6 MW, and the electron cyclotron resonance heating (ECRH) power is kept at 0.5 MW, while the line-averaged density increases from 2.5 to 3.3 $\times 10^{19}$ m^{-3}. Additionally, the stored energy is controlled in the 5% fluctuation range, which can be regarded as unchanged; thus, we suppose that the temperature of the plasma decreases. Figure 3(d) shows the raw data of the electron cyclotron emission (ECE) signal, which cannot be used as temperature data due to LHW heating, but the data in the position of $\rho \sim 0.76$ can respond to the trends of temperature

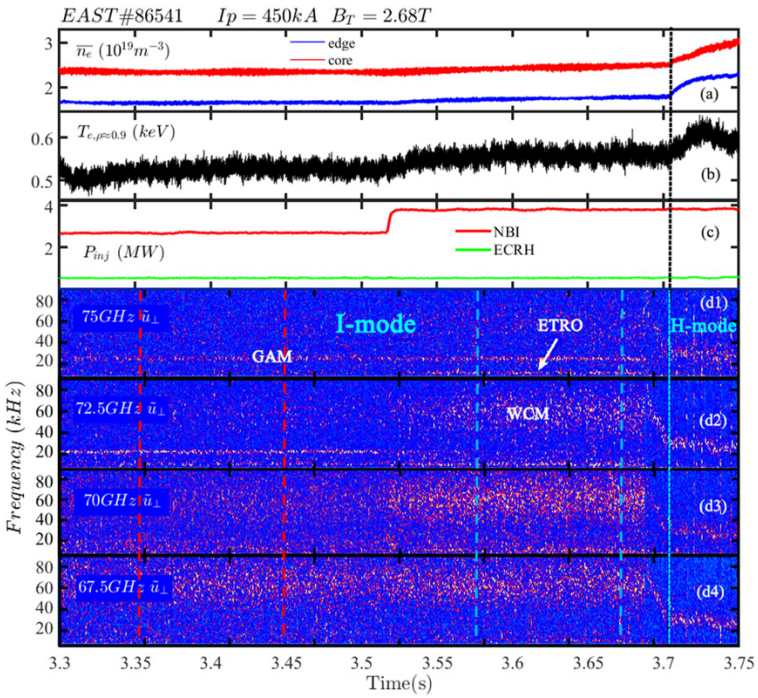

Figure 1. Typical I-mode in EAST under NBI and ECRH heating with an upper single null configuration. The dashed lines represent the I-mode and H-mode. (*a*) Line-averaged density $\bar{n_e}$. (*b*) Electron temperature at $\rho \sim 0.9$. (*c*) Injected power. (*d*) Time frequency spectrum for $\widetilde{u_\perp}$ from four positions, the sampling frequency for DR is 10^{-7} s.

changes in the pedestal range. Based on the above two points, we suggest that the temperature is decreasing from 2.7 s to 2.9 s.

Compared with the WCM of 2.7–2.72 s, the WCM of 2.9–2.92 s becomes much weaker, which is approximately opposite the trend of the increase in the density, i.e., approximately consistent with the downward trend of the temperature. Therefore, the intensity of the WCM is positively correlated with temperature. Both I-mode discharges shows the intensity of WCM is related to the state of I-mode plasma, but the triggering mechanism of the WCM and its effect in I-mode need further research; thus, some simulation studies were conducted.

3. Simulation result

To facilitate comparison with the results from the experiment, the original grid file is based on the experimental data with a $260 \times 64 \times 64$ mesh, while the radial range is $\rho = 0.85$–1.05. Due to large magnetic shear, magnetic flux surfaces are closely packed together, therefore a large number of radial grid point (nx) is needed to resolve the fine radial structures for different poloidal harmonics in the pedestal region. The previous paper [21] shows the simulation solutions converge well at $nz = 64$ for $\Delta N = 5$, which is the setting in our simulation work. The profiles for temperature and density input are obtained from experimental diagnosis, through the necessary smooth fitting shown in figure 4, the density and temperature profiles in SOL are assumed to be uniform, so there is no current in this region. In addition, the magnetic flux surfaces are obtained from the EFIT calculation of discharge #71078, has been reported in figure 3 of the first paper about I-mode discharges in EAST [13]. #71078 is a stable I-mode discharge, lasted for 4.5 s, it has relatively complete diagnostic data and is stable and lasting, thus it is used as a standard discharge of I-mode, also used for simulation here. We use the mature six-field model [23] in BOUT++ [24], which is based on Braginskii equations, within the flute reduction, the E_r is calculated by force balance, to simulate the development process of instability and the process of transport. We compare the results of the full six-field nonlinear simulation with the inclusion of various physics mechanisms: compressible terms, parallel velocity terms, energy exch, energy flux, gyro-viscousity, resistive ballooning, thermal force, the primary finding is that the DAW mode is the dominant term, as shown in figure 5, while the normalized growth rates only including other physics mechanisms are lower than 0.02 and can be regarded as stable. The DAW is driven by $\frac{1}{en_{e0}} \bigtriangledown_\parallel P_e + \frac{0.71 k_B}{e} \bigtriangledown_\parallel T_e$ in the time advance for $A_\parallel$, it can be seen that the electron pressure and temperature gradient plays a key role in the I-mode instability. In addition, I-mode characterized by low density gradient and high temperature gradient, hence the electron temperature gradient is the main instability source for I-mode.

The actual physical process cannot be the ideal linear process mentioned above, so a nonlinear simulation with the same grid file is carried out. For the optional physical terms of the

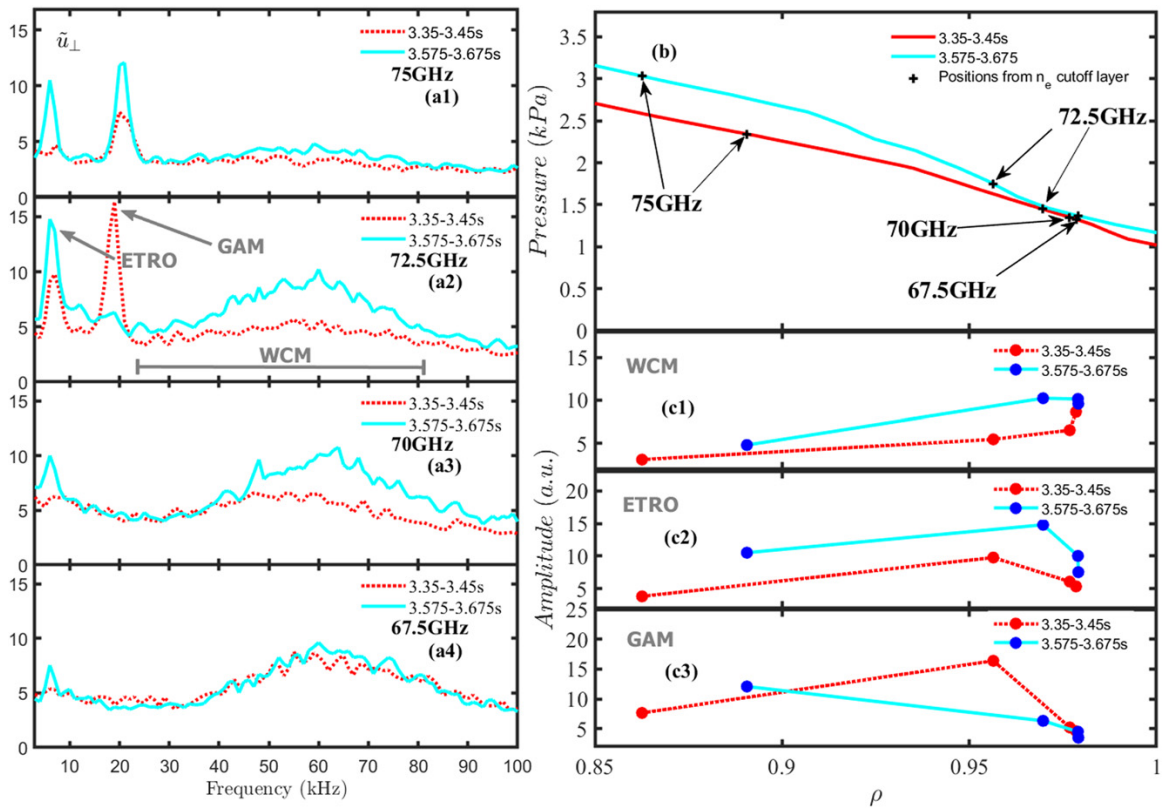

Figure 2. Detailed signals of shot 86541: (*a*) power spectrum of the $\widetilde{u_\perp}$ fluctuations. (*b*) The pressure for # 86541 and detailed positions corresponding to the four frequencies, the positions for 70 and 67.5 kHz are enlarged and painted in the lower left corner. (*c*) Peak amplitudes of the (1) WCM, (2) ETRO and (3) GAM.

nonlinear simulation, we compare the results of the full six-field simulation with those of the full six-field simulation without the DAW mode, which is the dominant term in the linear simulation. In the result of nonlinear simulation, the dominant toroidal mode is $n = 25$ (shown in figure 5(*b*)), while that of the linear result is $n = 50$ because the energy tends to have an inverse cascade toward a larger scale [26]. The spectrum analysis of the simulated density fluctuation is shown in figure 6. In the full six-field case, the eigenfrequency of the WCM (50 kHz for full six-field case) is approximately consistent with the results from the experiment (52 kHz), while there is no WCM in the case without the DAW mode. Furthermore, the calculation results of electron diffusivities are shown in figure 7, where the red line and blue line are the results with and without the DAW term during 962–1000 τ_A, respectively. The termination of the simulation depends on whether rmsu is reasonable, including if it has the singularity and whether its peak position corresponds to the gradient peak position of the evolutionary variable, so I choose the 1000 τ_A as the terminant time of this simulation. The corresponding simulation profiles are shown in figure 4, abscissas of the figures 4 and 7 are ρ and ψ respectively, $\rho = \sqrt{\psi}$, the top of gradient for profiles in figure 4 converted to ψ is where $\psi = 0.89$, it is close to the peak of the envelop of the transport coefficient as shown in figure 7. This indicates that the DAW mode helps improve transport and that the particle diffusivity is larger than the heat diffusivity in the temperature pedestal regime, which is consistent with the result from I-mode simulation transport of C-Mod [25].

Previous experimental results from C-Mod [27] also show that the WCM electron temperature fluctuation level is an order of magnitude smaller than the WCM density fluctuation level; hence, the WCM is believed to play a key role in increasing transport at the edge of I-mode plasmas. Based on the above results, a qualitative theoretical explanation for a basic physical mechanism of WCM maintaining the I-mode can be formed. First, the electron obtains energy from auxiliary heating power; thus, its temperature and temperature gradient increase. Then, the DAW modes are driven by the temperature gradient [28], which helps develop the WCM; thus, the density of plasma remains almost the same, while the temperature increases. Consequently, the WCM can help to sustain I-mode, featured low density and high temperature.

The density fluctuation is also obtained by the SymPIC code, which adopts an electromagnetic fully kinetic particle-in-cell scheme [3] based on a charge conservative geometric structure preserving discretization of the toroidal plasma. By exactly conserving the symplectic two-dimensional of the discrete particle-electromagnetic field system, this scheme

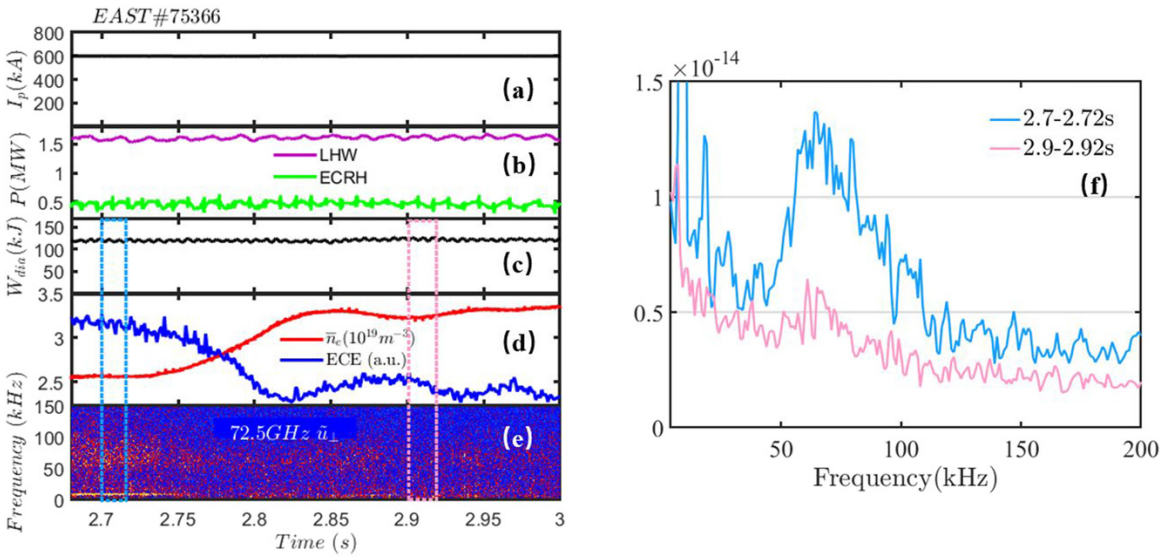

Figure 3. The 0.32 s I-mode discharge #75366, time traces of (*a*) plasma current; (*b*) auxiliary heating power; (*c*) stored energy $W_{\rm dia}$; (*d*) line-averaged density $\bar{n}_{\rm e}$ and ECE signal in $\rho \sim 0.76$; (*e*) time frequency spectrum for $\widetilde{u_\perp}$; and (*f*) power spectra of $\widetilde{u_\perp}$ for two time ranges.

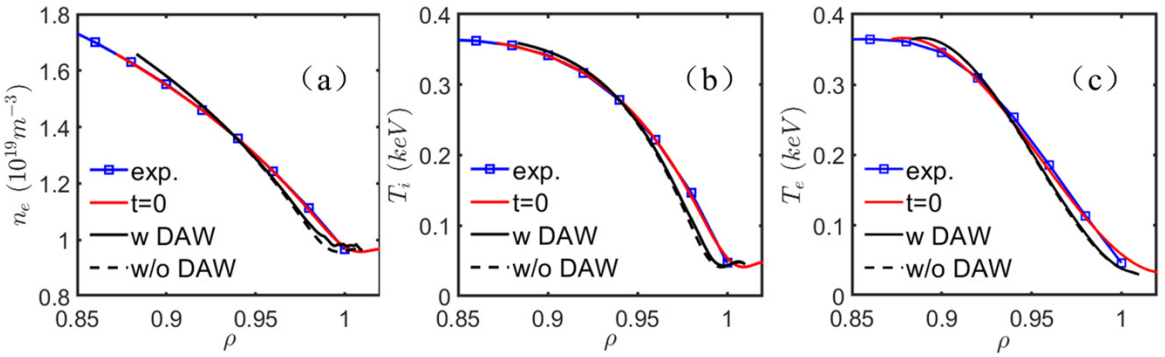

Figure 4. Profiles between the experimental fitted data ([13] figure 3 in 4.04 s) and simulated grid data for (*a*) $N_{\rm e}$; (*b*) $T_{\rm i}$ and (*c*) $T_{\rm e}$. The black lines are the fitted experimental data from #71078, the blue lines are the original profiles used in the BOUT++ simulation, the black dashed and dashed lines are simulation results in 1000 $\tau_{\rm A}$ of cases with and without DAW respectively.

can bind invariants such as the total energy and momentum by a small value during the long-term simulation. Compared with BOUT++ simulations, in SymPIC simulations, the kinetic effect and self-consistent radial electric field are naturally included, which may be crucial for the tokamak edge plasma. Simulation parameters can be briefly introduced as follows. The EAST plasma is discretized over an $R \times \Phi \times z = 192 \times 64 \times 192$ mesh, in which $R_{\rm left} = 1.274$, $\Delta R = 6.25 \times 10^{-3}$ m, $z_{\rm min} = 0.9625$ m, $\Delta z = 1.75\Delta R$, and $\Delta{\rm phi} = 2\pi/64$. Initially, outside the last closed flux surface for all three directions, the boundaries for fields and particles are set to perfect electric conductors and absorbing boundaries, respectively. The plasma is simply a deuterium–electron plasma, both densities are calculated by $n_{\rm i} = n_{\rm e} = P/(T_{\rm i} + T_{\rm e})$, and the masses of ions and electrons are set to $m_{\rm i} = 100m_{\rm e} = 3.34 \times 10^{-27}$ kg. The pressure P, initial plasma current density J and initial magnetic field B are given by EFIT from EAST experimental shot 71078 at 4.1 s. To reduce the numerical complexity, the numerical speed of light is reduced to $0.25c$, where $c = 299\,792\,458$ m s^{-1} is the real speed of light in vacuum. The time step is set to $\Delta t = 2\Delta R/c$, and the total number of time steps is 10^6. The field values are output each 5000 time-steps.

The preliminary nonlinear simulation results from SymPIC are shown in figure 8; the value ranges for the grid points of BOUT++ and SymPIC are shown in (*a*) and (*b*) respectively. And the BOUT++ six-field model is based on the Braginskii equation while the SymPIC model is based on the Vlasov–Maxwell equation. The power spectrum of density fluctuation for two approaches (BOUT++ and SymPIC) all show that the characteristics of the WCM (50 kHz for

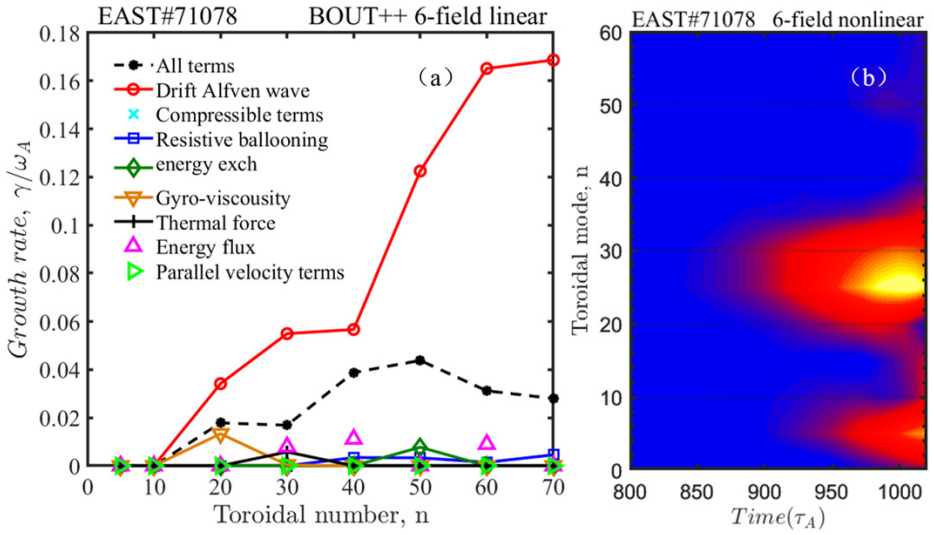

Figure 5. (*a*) Growth rate normalized by the Alfvén frequency versus the toroidal number n with different physical terms (only include the term described in legend). (*b*) Time-n (toroidal mode) spectrum.

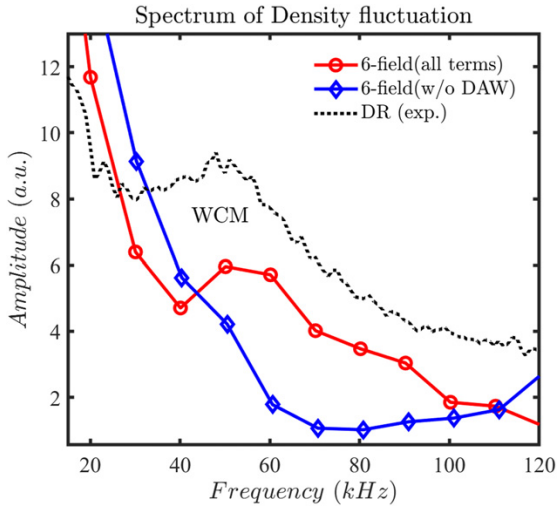

Figure 6. Power spectrum of the density fluctuations under three conditions: experimental data from the DR signal (black dashed line), all six-field nonlinear progress (red line) and all six-field without the DAW term (blue line).

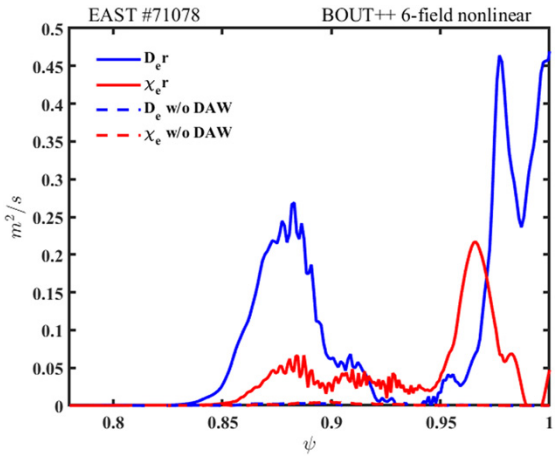

Figure 7. Profiles of the electron diffusivities of the full six-field with/without DAW mode calculated from the simulation results.

BOUT++ and 67 kHz for SymPIC) and the central frequency are comparable. We still obtain a similar central frequency; thus, the WCM conforms to the physical items in both models. As for the dominant mode in BOUT++ simulation result, i.e. the DAW, its effect is also reflected in SymPIC. SymPIC directly solves the dynamics of particle-electromagnetic fields system, which is the fundamental model for classical plasmas. The well-known Vlasov–Maxwell system with collisions is a reduction of the original particle-electromagnetic fields system, and the Braginskii equation is a fluid reduction of the collisional Vlasov–Maxwell system. The present Bout++ six-field simulation uses the model based on the drift ordering of the Braginskii equation, in which the DAW term, i.e. $\frac{1}{en_{e0}}\nabla_\parallel P_e + \frac{0.71k_B}{e}\nabla_\parallel T_e$ in the time advance for $A_\parallel$ [23], can be obtained from the Vlasov equation using the Chapman–Enskog theory, when the velocity distribution for electrons is near Maxwellian. So the effects introduced by the DAW term, although not explicitly presented in the original Vlasov–Maxwell equation, should be interpreted by the first-principle particle-in-cell simulation performed by the SymPIC, if the velocity distribution of electrons is near Maxwellian. We have verified that the velocity distribution of electrons in SymPIC simulations is indeed near Maxwellian, which indicates that effect of DAW should be exist. It should be noted that the thermal force effect in PIC simulations may be difference from that in fluid dynamics, but according to our tests it is not significant to effect the result.

In the future, we plan to further study the mode of instability turbulence of the I-mode based on the results from the SymPIC code.

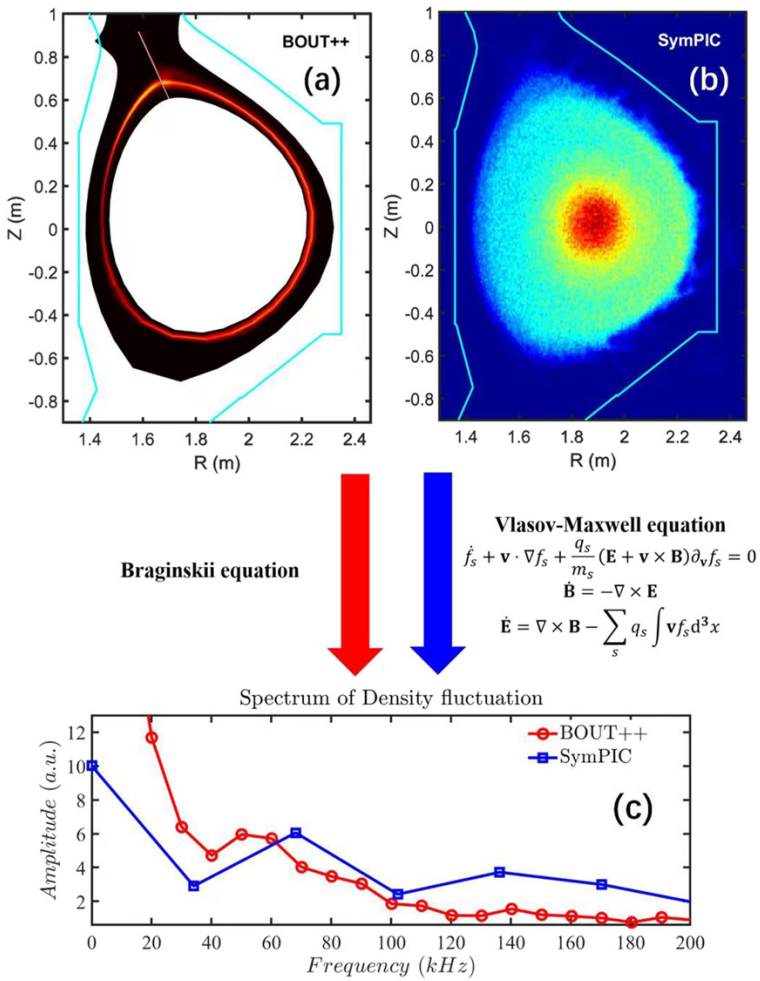

Figure 8. Top, value range of the grid for (*a*) BOUT++ and (*b*) SymPIC; below, power spectra of density fluctuation with two conditions: the full six-field BOUT++ program and the SimPIC program.

4. Summary and discussion

In summary, this paper reports the experimental results of EAST and simulation results based on experimental data. The experimental result shows that the WCM is accompanied by the I-mode, and its intensity is related to the electron temperature. In figure 1, the WCM enhanced with additional NBI injection and the I–H transition was delayed due to this enhanced WCM. The most reasonable explanation is that the WCM absorbs the energy for transiting to H-mode and sustains I-mode for some time. Without the I–H transition, just the redistribution of energy in proportion to temperature and density as shown in figure 3, the intensity of WCM shows a positive correlation with electron temperature. Additionally, the GAM and ETRO are observed simultaneously with WCM. The peak value of GAM moves away from the pedestal and weaken thus it is believed that it has little to do with the transport in the edge. As for the ETRO, it shows the same change trend as WCM, but the ETRO is somewhat more difficult to simulate due to its low frequency, and the frequency and amplitude make it an unlikely candidate for driving significant flux. Based on the two points above, firstly with the NBI power injecting, the amplitude of WCM increased and plasma maintain in I-mode; secondly the position of the amplitude of WCM increased most is in the pedestal range, thus the WCM helps retain the I-mode. Plus, the DAW is driven by gradient of electron temperature, and DAW drive WCM, it is also consistent with the phenomenon that WCM enhanced with increasing electron temperature observed in experiment.

Based on the I-mode boundary data of EAST, the BOUT++ program based on the two-fluid model and the SymPIC program based on the kinetic effect PIC model predict density turbulence values very close to the experimental results, which shows that these two models can explain the phenomena observed in our experiments to a certain extent. Through the simulation analysis using the relatively simple two-fluid model of BOUT++, we find that the DAW mode drives the WCM and that the transport is enhanced by the latter. As for the DAW in SymPIC code, although not explicitly presented in the original Vlasov–Maxwell equation,

should be interpreted by the first-principle particle-in-cell simulation performed by the SymPIC, if the velocity distribution of electrons is near Maxwellian. We have verified that the velocity distribution of electrons in SymPIC simulations is indeed near Maxwellian, which indicates that effect of DAW should be exist. It should be noted that the thermal force effect in PIC simulations may be difference from that in fluid dynamics, but according to our tests it is not significant to effect the result.

Acknowledgments

This work was supported by the National Magnetic Confinement Fusion Program of China under Contract Nos. 2019YFE03090200, 2018YFE0311200 and 2019YFE03090200 and by the National Natural Science Foundation of China under Contract Nos. 11975230, 11975231 and 12175277, Collaborative Innovation Program of Hefei Science Center, CAS under Contract No. 2021HSC-CIP018. This work was performed under the U.S. Department of Energy by Lawrence Livermore National Laboratory under Contract No. DE-AC52-07NA27344, LLNL-JRNL-844653

References

[1] Xiao J., Qin H. and Liu J. 2018 *Plasma Sci. Technol.* **20** 110501
[2] Xiao J., Qin H., Liu J., He Y., Zhang R. and Sun Y. 2015 *Phys. Plasmas* **22** 112504
[3] Xiao J. and Qin H. 2021 *Plasma Sci. Technol.* **23** 055102
[4] Whyte D.G. *et al* 2010 *Nucl. Fusion* **50** 105005
[5] Hubbard A.E. *et al* 2016 *Nucl. Fusion* **56** 086003
[6] Loarte A. *et al* 2014 *Nucl. Fusion* **54** 033007
[7] Ryter F. *et al* 1998 *Plasma Phys. Control. Fusion* **40** 725
[8] Liu Y.J. *et al* 2020 *Nucl. Fusion* **60** 082003
[9] Hubbard A.E. *et al* 2017 *Nucl. Fusion* **57** 126039
[10] Happel T. *et al* 2017 *Plasma Phys. Control. Fusion* **59** 014004
[11] Marinoni A. *et al* 2015 *Nucl. Fusion* **55** 093019
[12] Cziegler I. 2017 *Phys. Rev. Lett.* **118** 105003
[13] Feng X. *et al* 2019 *Nucl. Fusion* **59** 096025
[14] Ryter F. *et al* 2017 *Nucl. Fusion* **57** 016004
[15] White A.E. *et al* 2014 *Nucl. Fusion* **54** 083019
[16] Manz P., Happel T., Stroth U., Eich T. and Silvagni D. 2020 *Nucl. Fusion* **60** 096011
[17] Viezzer E. *et al* 2013 *Nucl. Fusion* **53** 053005
[18] McDermott R.M. *et al* 2009 *Phys. Plasmas* **16** 056103
[19] Liu X. 2018 Gyrokinetic simulation of pedestal turbulence using GENE *PhD Thesis* University of Texas
[20] Liu A.D. *et al* 2020 *Nucl. Fusion* **60** 126016
[21] Xu X.Q., Dudson B.D., Snyder P.B., Umansky M.V., Wilson H.R. and Casper T. 2011 *Nucl. Fusion* **51** 103040
[22] Hu J.Q. *et al* 2017 *Rev. Sci. Instrum.* **88** 073504
[23] Xia T.Y., Xu X.Q. and Xi P.W. 2013 *Nucl. Fusion* **53** 073009
[24] Dudson B.D., Umansky M.V., Xu X.Q., Snyder P.B. and Wilson H.R. 2009 *Comput. Phys. Commun.* **180** 1467
[25] Liu Z.X. *et al* 2016 *Phys. Plasmas* **23** 120703
[26] Scott B.D., Biglari H., Terry P.W. and Diamond P.H. 1991 *Phys. Fluids* B **3** 51
[27] White A.E., Phillips P., Whyte D.G., Hubbard A.E., Sung C., Hughes J.W., Dominguez A., Terry J. and Cziegler I. 2011 *Nucl. Fusion* **51** 113005
[28] Ma J. 2015 The macro- and micro-instabilities in the pedestal region of the tokamak *PhD Thesis* University of Texas